Northumbria Research Link

Citation: Khiam, Goh Kheng, Karri, Rama Rao, Mubarak, Nabisab Mujawar, Khalid, Mohammad, Walvekar, Rashmi, Abdullah, Ezzat Chan and Rahman, Muhammad (2022) Modelling and optimization for methylene blue adsorption using graphene oxide/chitosan composites via artificial neural network-particle swarm optimization. Materials Today Chemistry, 24. p. 100946. ISSN 2468-5194

Published by: Elsevier

URL: https://doi.org/10.1016/j.mtchem.2022.100946 <https://doi.org/10.1016/j.mtchem.2022.100946>

This version was downloaded from Northumbria Research Link: https://nrl.northumbria.ac.uk/id/eprint/49303/

Northumbria University has developed Northumbria Research Link (NRL) to enable users to access the University's research output. Copyright © and moral rights for items on NRL are retained by the individual author(s) and/or other copyright owners. Single copies of full items can be reproduced, displayed or performed, and given to third parties in any format or medium for personal research or study, educational, or not-for-profit purposes without prior permission or charge, provided the authors, title and full bibliographic details are given, as well as a hyperlink and/or URL to the original metadata page. The content must not be changed in any way. Full items must not be sold commercially in any format or medium without formal permission of the copyright holder. The full policy is available online: http://nrl.northumbria.ac.uk/policies.html

This document may differ from the final, published version of the research and has been made available online in accordance with publisher policies. To read and/or cite from the published version of the research, please visit the publisher's website (a subscription may be required.)

Northumbria University NEWCASTLE

University Library

Modelling and optimization for methylene blue adsorption using graphene oxide/chitosan composites via artificial neural network -particle swarm optimization

Goh Kheng Khiam[1], Rama Rao Karri[2*], N.M. Mubarak[2]*, Mohammad Khalid[3*], Rashmi Walvekar[4], Ezzat Chan Abdullah[5], Muhammad Ekhlasur Rahman[6]

[1] Department of Chemical Engineering, Faculty of Engineering and Science, Curtin University, 98009 Miri Sarawak, Malaysia

[2] Petroleum, and Chemical Engineering, Faculty of Engineering, Universiti Teknologi Brunei, Brunei Darussalam

[3] Graphene & Advanced 2D Materials Research Group (GAMRG), School of Engineering and Technology, Sunway University, 47500 Petaling Jaya, Selangor, Malaysia

[4] Department of Chemical Engineering, School of Energy and Chemical Engineering, Xiamen University Malaysia, Jalan Sunsuria, Bandar Sunsuria, 43900, Sepang, Selangor, Malaysia

[5] Department of Chemical Process Engineering, Malaysia–Japan International Institute of Technology (MJIIT) Universiti Teknologi Malaysia (UTM), Jalan Sultan Yahya Petra, 54100, Kuala Lumpur, Malaysia

[6] Department of Mechanical & Construction Engineering at Northumbria University, Newcastle upon Tyne, United Kingdom

*Corresponding authors: kramarao.iitd@gmail.com (Rama Rao Karri); mubarak.yaseen@gmail.com (N.M. Mubarak); khalids@sunway.edu.my (M. Khalid)

Abstract

Water pollution due to dyes from industrial effluents and domestic wastewater is a big environmental issue, so an effective adsorbent is needed. In this study, graphene oxide/chitosan (GO/CS) composites were synthesized and applied for methylene blue (MB) dye removal. Characterization was done on the GO and GO/CS composites using FTIR, EDX, SEM, and TGA. The adsorption studies were conducted to verify the effect of pH, adsorbent dosage and contact time. The interactive effects of the process variables were verified using response surface methodology (RSM), and optimal conditions for higher adsorption efficiency are evaluated by Artificial neural network (ANN)-Particle swarm optimization (PSO). ANN-PSO

predictions are in good agreement with the experimental values and hence resulted in higher R^2 (=0.998) compared to RSM predictions (R^2 = 0.981). The MB adsorption process is found to be obeying the Langmuir isotherm and pseudo 1st order kinetic model. The maximum MB removal efficiency (90.34%) and adsorption amount (7.53 mg/g) can be obtained at an initial dye concentration of 10 mg/L and optimal values of pH (5), adsorbent dosage (0.143 g/L) and contact time (125 min). These results further confirm that the ANN-PSO-based approach is able to capture the inherent mechanisms of the MB adsorption process and can be used as a good modelling approach.

Keywords: Graphene oxide/chitosan composite; Methylene blue; Response surface methodology; Particle swarm optimization; Artificial neural network

1. Introduction

A huge amount of dyes is being used in the textile industry every year, and the excess dyes are carried with water used for cleaning. The textile industry alone contributes huge quantity of dye wastewater annually [1]. In the present era, the dyes used in the textile industry are mostly synthetic dyes rather than natural dyes. This is due to the limited availability of natural dyes and fading of color when exposed to sunlight during drying [2]. According to the world bank [3], the effluent from the textile industry contains 72 toxic chemicals; among these, 30 chemicals are difficult to be removed from wastewater using the treatment process [4]. The effluent of the textile industry contains heavy metals and toxic chemicals like cyanide, oil, and grease [5]. More synthetic chemicals are manufactured and used widely in these textile industries due to their improved stability at high temperatures and UV radiation [6]. The dye wastewater that consists of various hazardous chemicals poses a severe danger to the environment, animals, and humans and hence needs proper removal treatment. These pollutants can accumulate in soil and pose long-term danger [7-9]. In this regard, many countries have enforced laws and regulations to control the effluent from the textile industry. International

standards for dye effluent are biological oxygen demand (BOD) (<30 mg/L), chemical oxygen demand (COD) (<50 mg/L), colourless, pH (6-9), suspended solids (<20 mg/L), temperature (<42°C) [10-12]. However, some industrial plants violate the laws leading to water pollutions.

Recently, graphene has been getting worldwide attention for its extraordinary chemical, physical, thermal and electrical properties [13, 14]. Its role as a filler in a polymer matrix to form nanocomposites has dramatically improved the mechanical and thermal properties compared to graphite-based composites [15]. Graphene is a 2D structure formed by a single sheet of carbon atoms arranged in a honeycomb shape, while graphite refers to stacks of graphene planes arranged in hexagonal or rhombohedral sequence [16]. In graphene, sp^2 hybrids form σ bonds which contribute to the extremely high Young's modulus of 1 TPa. Graphene can be obtained from graphite by ultrasound sonication treatment, where the multilayer structure of graphite sheets can be exfoliated to make graphene [16].

On the other hand, graphene oxide (GO) is formed when graphene is oxidized. The functional groups of the oxidant for the oxidation process can be hydroxyl (OH), carbonyl (C=O), and alkoxy (C-O-C). The degree of oxidation or the grades of oxidation is dependent on the number of oxygen present in the structure of GO. When the GO has a percentage of oxidation ranging between 0-10 %O, this GO is termed as reduced graphene oxide (rGO) [17]. Theoretically, the maximum oxidation that GO can achieve is 50 %O due to the sp^2 hybridization of carbon atoms in graphene hexagons [18].

Chitin, the second most abundant source of natural biopolymer on earth, can be obtained from both plants and animals [19, 20]. It is commonly found in the cell wall of fungi, yeast, and the shell or exoskeleton of insects and sea animals. The percentage of chitin in different sources ranges from 3 - 40%. Chitin has a similar structure to cellulose as both of these biopolymers are in the class of polysaccharides; their difference is that the acetamide group exists in chitin . It is biodegradable, biocompatible, non-toxic, renewable, and affordable, thus

making this biopolymer more advantageous in biomedical and pharmacological applications. Chitosan, the most important derivative of chitin, is insoluble in water; however, it is soluble in acidic conditions. Chitosan (CS) also possesses significant features like biodegradability, biocompatibility, nontoxicity, antibacterial activity, and strong film-forming features. Recently, chitosan has been vastly researched by the scientific community and applied in a wide range of applications, for instance, water and wastewater treatment and biomedical [21, 22]. Due to its excellent biodegradability and biocompatibility, chitosan is labeled as a green adsorbent. Also, its adsorption efficiency is not broad; the hydroxyl and amine groups of chitosan behave as active sites to store anionic pollution, but its inclination towards cationic dyes is slight because of its adverse electrostatic interactions. But, when evaluated as a composite with GO, chitosan-based material attained removal of a minimum of 85% for cationic dyes [23].

Besides, GO embedded in chitosan is an active technique for enhancing chitosan's physical and chemical properties. Several research studies have incorporated GO with chitosan (low concentrations) to produce strong, biocompatible, and biodegradable graphene oxide/chitosan (GO/CS) nanocomposites. This is due to the strong interaction between GO and chitosan. Adequate diffusion of GO in chitosan matrix on a molecular scale, and interfacial adhesion, consequently substantially improving properties of GO/CS nanocomposites [24]. Sabzevari et al. [25], in their study, crosslinked GO with CS and their studies confirmed that the adsorption properties of GO are markedly improved upon the formation of a GO–chitosan composite. Another recent study by Muda et al. [26] applied GO-CS for rotenone pesticide removal. In their studies, they found that the CS-GO nanocomposites possess ideal characteristics as nanocarriers for hydrophobic rotenone and can be used as water-solubilizing agents so that the pesticides can become eco-friendly & safer for the environment. Hence, intending to produce a material that can be competitive with cationic dyes, with superior morphology, mechanical adsorption properties, the research on GO/CS composites has attained considerable momentum.

Furthermore, the majority of the studies mentioned above did not focus on optimizing the adsorption process parameter, which affect the removal efficiency using statistical modelling. It is very important to design experiments and optimize limited resources to reduce time and ambiguity in the results. The design of experiments using a novel approach such as response surface methodology (RSM); reduces the wastage of valuable chemicals, minimizes the experimental time, and thus leads to the effective use of experiment runs [17, 27-29].

To predict the process conditions at which it results in maximum performance, a data-driven model based on an artificial neural network (ANN) is a very useful approach. ANN needs no introduction, and it has been extensively used in all fields of engineering and sciences. In recent years, ANN is integrated with hybrid evolutionary techniques like a genetic algorithm (GA) [30], differential evolution optimization (DEO) [31], particle swarm optimization (PSO) [32], ant colony optimization (ACO) [33, 34], etc. These hybrid evolutionary techniques optimize the weights in the hidden layer. Owing to the benefits of PSO, which mimics the behavior of birds and is found to be successfully applied in diverse fields [32, 35].

Considering the immense benefits of graphene oxide and Chitosan and addressing the issue of dye removal, graphene oxide/chitosan composite is synthesized. Therefore, the main objective of this is to synthesize and evaluate the performance of graphene oxide/chitosan composite to remove the cationic dye, MB, from aqueous solutions. To conduct a minimum number of experiments and optimize the process variables RSM with Box-Behnken Design (BBD) framework is used. To predict the MB dye removal at different process conditions, a data-driven model based on an artificial neural network (ANN) embedded with particle swarm optimization (PSO) is used. The implementation of optimization methodologies and a data-driven strategy to forecast MB dye removal using the graphene oxide/chitosan composite has never been published in the open literature, thus making this work unique.

2. Materials and Methods

2.1 Materials

The materials used were graphene powder (8 nm flakes), 360 mL of sulfuric acid (H_2SO_4) (95-97% purity), 40 mL of phosphoric acid (H_3PO_4) (50%), 50 mL of humic acid colloid, 18 g of potassium permanganate ($KMnO_4$) (99% purity), 3 mL of hydrogen peroxide (H_2O_2) (30%), 200 mL of hydrochloric acid (HCl) (30%), sodium hydroxide (NaOH) (99%), 8 mL of acetic acid (CH_3COOH) (99%), low molecular weight chitosan powder (50,000-190,000 Da), methylene blue powder, 400 mL of ice and 2000 mL of ultrapure water. All chemicals were purchased from Sigma-Aldrich and used as received without further purification.

2.2 Apparatus and Equipment

The equipment used in this experiment were probe ultra-sonicator (LPS-500, SONO Mechanics), freeze dryer (Labconco), pH meter (HACH), centrifuge (Universal 320 R, Hettich), shaking incubator (SASTEC), ultra-pure water instrument (Purelab), Fourier-transform infrared spectrometer (FTIR, Perkin Elmer Frontier), field emission scanning electron microscopy (FESEM, FEI Quanta 400), energy-dispersive X-ray spectroscopy (EDX, FEI Quanta 400) and thermogravimetric analyzer (TGA, Perkin Elmer STA 6000).

2.3 Experimental Methods

2.3.1 Synthesis of GO

The synthesis of GO is based on the improved Hummer method [36]. Firstly, concentrated H_2SO_4 and H_3PO_4 with a ratio of 9:1 (360:40 mL) were mixed and added with 3 g of graphene powder and 18 g of $KMnO_4$. The mixing of these chemicals produced a slight exothermic reaction raising the temperature to 30 to 40°C. The mixture was stirred for 12 h at 50°C. Then cooling of the mixture was commenced until it reached room temperature and then poured into a beaker with an ice bath. Later, 3 mL of H_2O_2 was added to the mixture. The mixture was centrifuged at 4000 rpm for 30 min, and the supernatant layer was discarded. 200

mL of ultrapure water and 200 mL of 30% HCl were added to the solid residue. The mixture was centrifuged again at 4000 rpm for 30 min, and the supernatant layer was also discarded. This step was repeated at least four times with the same amount of ultrapure water and HCl for washing the solids. The solids, after washing, were transferred into smaller tubes and kept in the freezer. The frozen solids were freeze-dried using a freeze dryer at -50°C and vacuum condition for 24 h.

2.3.2 Synthesis of GO/CS composites

The GO powder and Chitosan were prepared with a weight ratio of 0.1 g:1 g (GO: CS). 0.1 g of GO was dissolved into 100 mL of ultrapure water and treated with an ultrasonic bath for 15 min to form a homogenous suspension of GO solution. 1 mL of humic acid colloid (HAC) and 1.0 g of Chitosan was added to 100 mL of ultrapure water. The Chitosan was stirred at room temperature until it completely dissolved into the solution. The chitosan solution and GO solution were mixed and stirred for 12 h. The mixture was frozen and freeze-dried at -50°C for 24 h. The GO/CS composites with a weight ratio of 0.2g (w/w) and 0.3g (w/w) were prepared in a similar way, and the amount of ultrapure water to dissolve both GO and CS was kept constant at 100ml each. The composites were labeled as GO/CS1, GO/CS2, and GO/CS3 for the weight ratio of 0.1g (w/w), 0.2g (w/w) and 0.3g (w/w) respectively. The 10 mg/L initial MB concentration was used to optimize the process parameter using RSM. The beaker was shaken at a specific agitation speed, and aliquots were collected from the reaction mixtures at specific time intervals. The mixture was diluted with distilled water, filtered through Whatman filter paper (42), and then sucked through a hydrophilic Polytetrafluoroethylene (PTFE) membrane using a vacuum pump (Brand: ULVAC. Model: DTC-41B). The absorbance was monitored at 595 nm using a UV-Vis spectrophotometer, and the MB concentrations were determined using a UV-Vis spectrophotometer. The MB dye removal efficiency (R%) was evaluated by using Equation (1):

$$\boldsymbol{R\%} = \left(\frac{\boldsymbol{C_0 - C_f}}{\boldsymbol{C_0}}\right) \times \mathbf{100} \quad (1)$$

Where C_0 and C_f are the initial and final concentration of MB dye, respectively

2.4 Design of experiments methodology

From previous similar studies, it was found that the pH, adsorbent dosage and contact time are the parameters that influence the MB removal [32, 37, 38]. As reported by most researchers, these process parameters are mostly used for dye removal studies by adsorption. Several experiments are to be conducted to understand the effect of each parameter on the overall MB removal efficiency. In the pH study, only acidic conditions of dye solution at pH 3, 4, 4.5 and 5 were studied, dosage the amount of adsorbent studied were 0.05 g, 0.75 g, 0.10 g and 0.15 and Initial concentration of 10 mg/L. These ranges are chosen based on the previous studies [32, 37, 38]. The agitation speed and temperature in these studies were set to be constant at 25°C and 100 rpm. A batch adsorption experiment was performed by using 100 mL of 10 mg/L of initial MB concentration to optimize the process parameters using the Design of Experiment as shown in ***Table* 1**. The effectiveness of dye removal is measured by percentage removal of dye and adsorption capacity or adsorption amount of adsorbent (amount of dye adsorbed per gram of adsorbent). In this regard, the design of experiments (DOE) methodology is used to estimate the experimental matrix, as shown in ***Table* 1.** Here, the Box-Behnken Design approach is applied, resulting in 17 experiments for the given set of process variables. So, as per the experimental matrix shown in this table, the corresponding experiments are conducted to determine the MB removal efficiency. This experimental matrix will also provide valuable information on the interaction effects of process variables and their impact on the overall removal efficiency. All adsorption experiments were done in triplicate, and the average values were used for further analysis.

Table 1. Design matrix by Box-Behnken design with three factors and two responses*

Run	*A: pH*	*B: Adsorbent dosage (g/L)*	*C: Contact time (min)*	*Response 1: MB Removal (%)*	*Response 2: Adsorption amount (mg/g)*
1	4 (0)	0.05 (-1)	120 (-1)	23.48	2.43
2	5 (+1)	0.05 (-1)	150 (0)	31.08	2.99
3	4 (0)	0.15 (+1)	180 (+1)	73.56	6.14
4	5 (+1)	0.10 (0)	180 (+1)	69.93	5.88
5	4 (0)	0.10 (0)	150 (0)	44.76	4.01
6	4 (0)	0.10 (0)	150 (0)	44.76	4.01
7	4 (0)	0.10 (0)	150 (0)	44.76	4.01
8	5 (+1)	0.15 (+1)	150 (0)	81.08	6.70
9	4 (0)	0.10 (0)	150 (0)	44.76	4.01
10	3 (-1)	0.10 (0)	120 (-1)	31.67	3.04
11	4 (0)	0.15 (+1)	120 (-1)	58.19	5.00
12	3 (-1)	0.15 (+1)	150 (0)	66.47	5.62
13	4 (0)	0.05 (-1)	180 (+1)	31.08	2.99
14	3 (-1)	0.10 (0)	180 (+1)	53.13	4.63
15	3 (-1)	0.05 (-1)	150 (0)	22.21	2.33
16	4 (0)	0.10 (0)	150 (0)	44.76	4.01
17	5 (+1)	0.15 (+1)	180 (+1)	85.39	7.02

** coded values in brackets*

2.5 A data-driven model developed using ANN-PSO

Due to the immense benefits of ANN and PSO in this research study, the ANN-PSO framework is used to develop the data-driven model to predict MB dye removal. The implementation procedure of ANN-PSO, its benefits, and evaluation of parameters was reported in the previous study [39]. In this research study, the process variables (pH, adsorbent dosage, and contact time) are used as inputs to the ANN-PSO framework, and response (MB removal %) is obtained as output from this model. The schematic representation of ANN-PSO Architecture, along with the input layer, hidden layer and output layer, is shown in ***Figure 1***. The model is trained, tested and validated using the 70%-15%-15% rule.

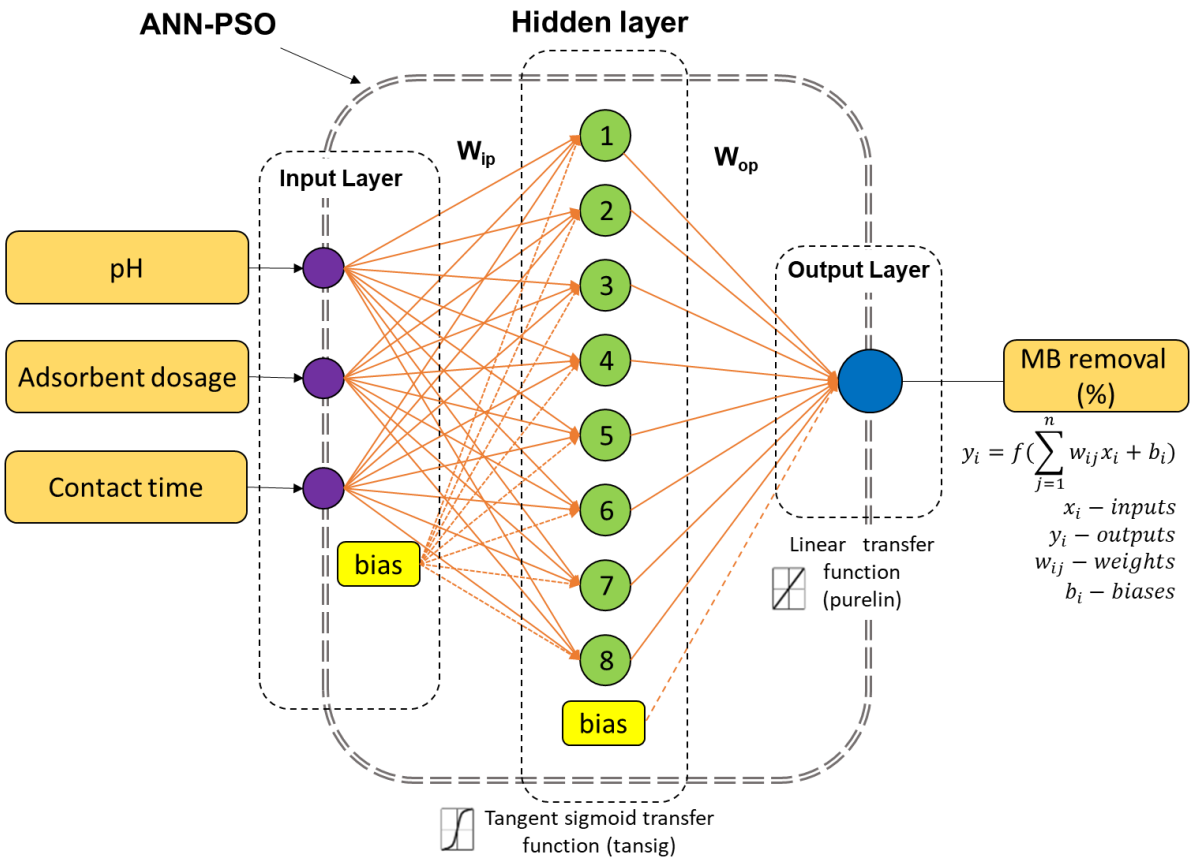

***Figure 1*:** Schematic representation of ANN-PSO Architecture

3. Result and Discussion

3.1 Characterization of GO/CS

3.1.1 Fourier-Transform Infrared Spectroscopy (FTIR) analysis

Fourier-Transform Infrared Spectroscopy (FTIR) is a technique to identify the organic compounds in a substance. A graph of transmittance versus wavelength is generated from this characterization technique. The stretching or peaks at a different wavelength and existing organic compounds are identified from the graph. The FTIR graph of GO, GO/CS1, GO/CS2, and GO/CS3 is shown in ***Figure 2***. From the graph, peaks can be seen, and the organic compounds represented by the peaks are identified. At a wavenumber of 3000 to 3500 cm^{-1}, the stretching vibration can be observed in the plot of GO, GO/CS1, and GO/CS2, which corresponds to the OH bonds. In the wavenumber range of 2800 to 3000 cm^{-1}, peaks can be seen in all four plots, and these bands are attributed to C-H bonds of CH_2 and CH_3 [40]. The

plot of GO, GO/CS1 and GO/CS2 have similar peaks at 1731 cm^{-1} and 1623 cm^{-1}. The peak at 1731 cm^{-1} corresponds to the C=O stretching vibration of carboxylic and carbonyl groups [41, 42]. The peak at 1623 cm^{-1} corresponds to the carbon-carbon bond of graphene [42]. Bands are observed at 1045 cm^{-1}, 1044 $cm^{-1,}$ and 1040 cm^{-1} for GO, GO/CS1, and GO/CS2, respectively. These three bands corresponding to the stretching vibration of C-O-C bonds alkoxy groups (epoxy) [43].

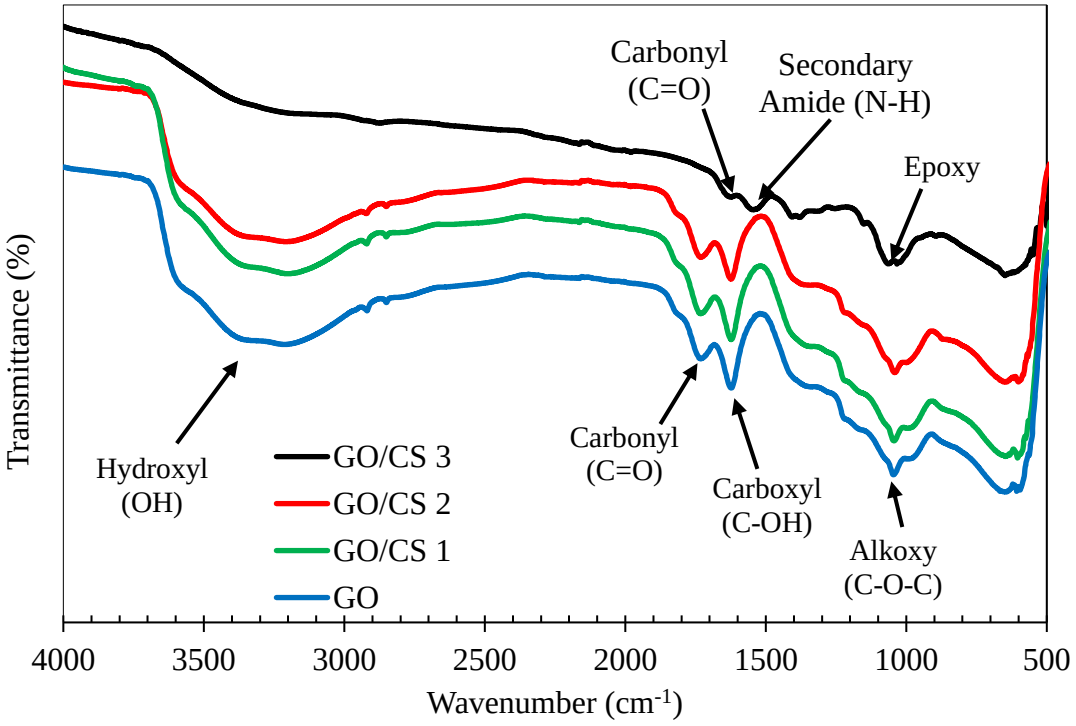

Figure 2: FTIR spectra of GO, GO/CS1, GO/CS2, and GO/CS3

However, the profile of GO/CS3 is slightly different when compared to the other three graphs. In the plot of GO/CS3, peaks are found at 1624 cm^{-1}, 1546 cm^{-1}, 1406 cm^{-1}, 1379 cm^{-1}, 1151 cm^{-1}, 1065 cm^{-1}, and 1033 cm^{-1}. The band at 1624 cm^{-1} is attributed to the C=O bonds carbonyl groups of NHCO or secondary amide (Amide II band) due to chitosan [44]. The band at 1546 cm^{-1} is attributed to the stretching vibration of N-H bonds of Amide II and the symmetric NH^{3+} deformation, and this band can also attribute to skeletal vibration of carbon-carbon bond in GO [44]. The bands at 1406 cm^{-1} and 1379 cm^{-1} correspond to the stretching vibration of O-H bonds of carbonyl groups and symmetrical deformation of CH_3 in the

acetamide group ($NHCOCH_3$), respectively [44-46]. At 1151 cm^{-1}, the stretching vibration corresponds to C-O-C antisymmetric. The band at 1065 cm^{-1} is attributed to N-H stretching vibration, while the band at 1033 cm^{-1} is attributed to the introduction of epoxy groups of graphene oxide [47]. From the result of FTIR, the composites of GO/CS1 and GO/CS2 do not bind well, which is why they have similar peaks to GO. In the peaks of GO/CS3, more bonds or amide groups can be identified, and Chitosan is the source of the amide group's bond. However, the peaks of GO/CS3 are very weak, which indicates that not much Chitosan is bound with GO.

3.1.2 Field Emission Scanning Electron Microscopy (FESEM) Analysis

Field emission scanning electron microscopy (FESEM) analysis was used to study the surface morphology of GO, GO/CS1, GO/CS2, and GO/CS3. ***Figure 3*** shows the SEM images of GO, GO/CS1, GO/CS2, and GO/CS3 at 5000 times magnification *(Figure S1 at 600 times magnification).* From ***Figure 3*** (a), the 2D structure of the GO sheet can be observed, and the surface of the composite becomes rougher when the composition of the GO and chitosan increases. The roughness on the surface is due to the crosslinking or entanglement of the graphene oxide and Chitosan [48]. This entanglement of the composite increased the surface area and thus improved the efficiency of the adsorption process. The surface morphology of GO/CS also shows that it has more pores, resulting in better adsorption.

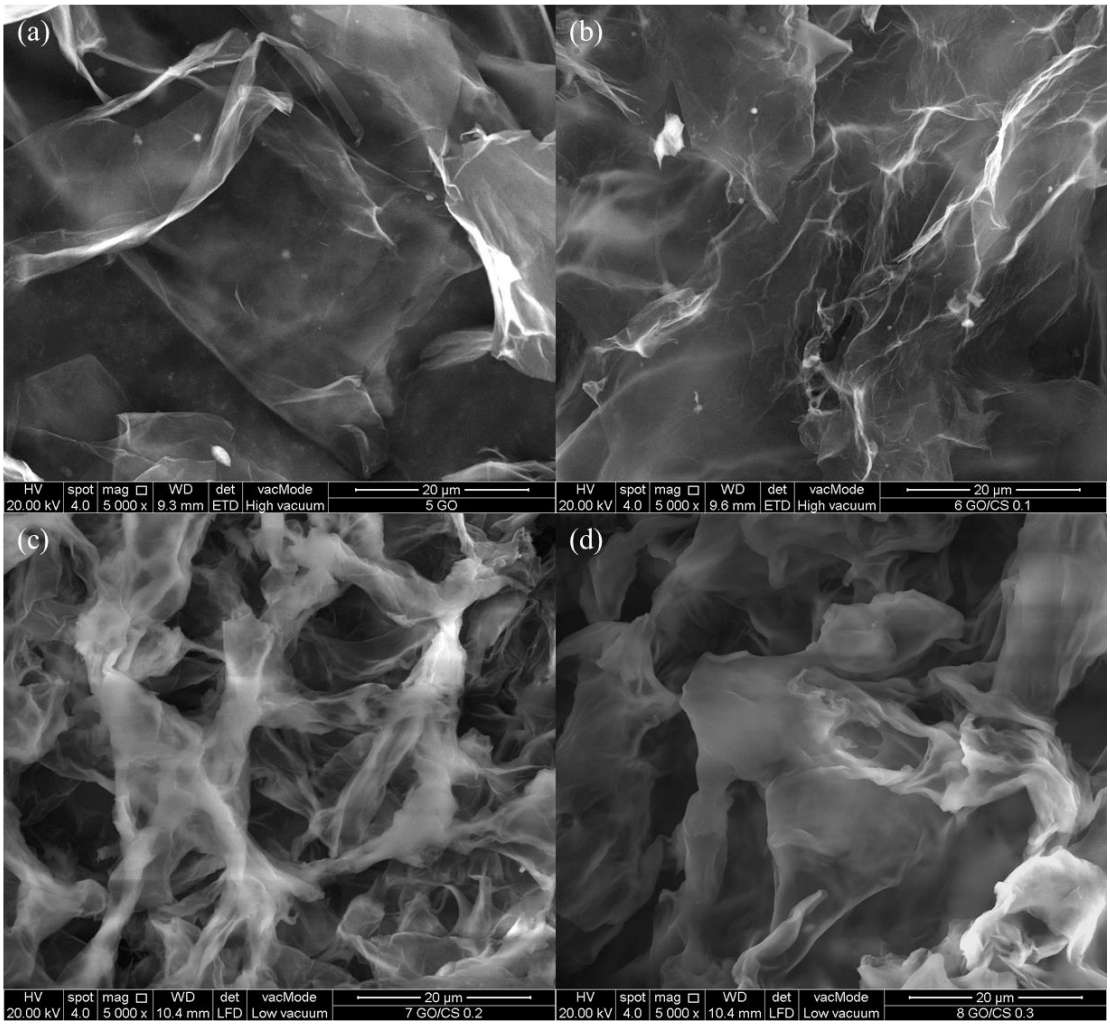

Figure 3 : FESEM images of (a) GO, (b) GO/CS1, (c) GO/CS2 and (d) GO/CS3 at magnification of 5000x

3.1.3 Energy-dispersive X-ray Spectroscopy (EDX) Analysis

Energy-dispersive X-ray spectroscopy (EDX) was carried out with FESEM. The resulting graph of EDX is shown in ***Figure 4***. The analysis was carried out at 2500 times magnification and acceleration voltage of 20kV. From the result of the EDX analysis, the percentage of N in GO/CS1, 2, and 3 are 3.81%, 3.82%, and 16.83%, respectively. The percentage of N increases with the amount of Chitosan used; this indicates that more Chitosan was successfully crosslinked with graphene oxide [45]. However, S and Cl are also found in the composites, and this is due to the usage of hydrochloric acid and sulfuric acid in the synthesis of GO which was not thoroughly washed off.

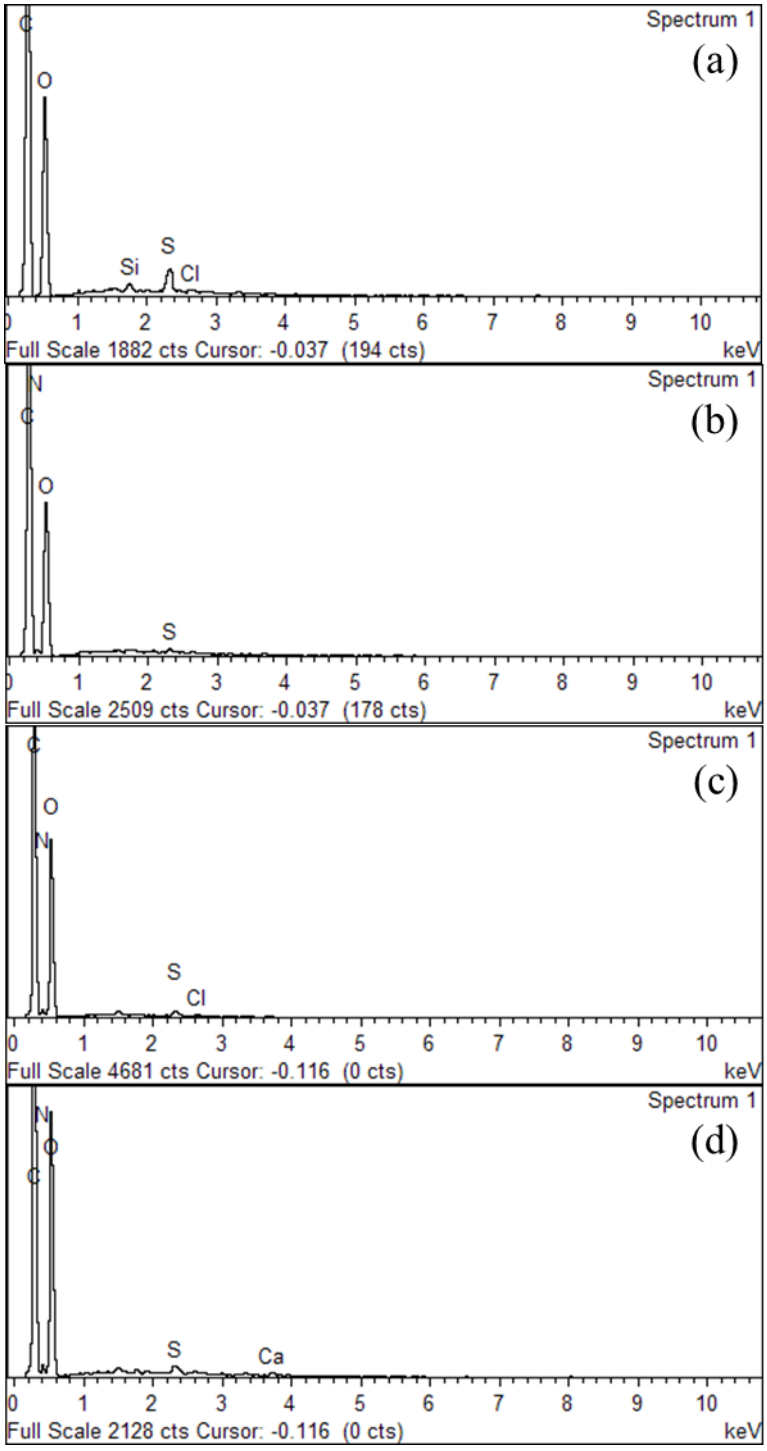

274

275 ***Figure 4*** : EDX analysis of (a) GO, (b) GO/CS1, (c) GO/CS2 and (d) GO/CS3

276

3.1.4 Thermogravimetric Analysis (TGA)

From the TGA curves (*see* ***Figure S2***) of GO/CS1, GO/CS2 and GO/CS3, three significant stages of weight loss can be seen at a temperature of 50°C, 140°C, and 230°C, respectively. Meanwhile, the loss of weight of GO has only two stages, at 50°C and 170°C. At 50°C, weight loss is due to the evaporation of water that is physically and chemically bonded with the composites. The weight loss between 140°C and 230°C is presumed to be due to the decomposition of oxygen functionalities of GO in the composites [49, 50]. These results indicate that the composites are much more thermally stable than the GO because of amino groups in the Chitosan [51].

3.2 Analysis of various process parameters on dye removal efficiency

3.2.1 Effect of pH

In this research study, four different amounts of adsorbent dosage and pH were used for removing methylene dye over three hours, and the percentage removal and adsorption capacity of the adsorbent were calculated and recorded every 30 min. The results of the study of pH are shown in ***Figure 5 (a)***. The data of percentage removal for the studies used for the graphs are the percentage of removal after 3 h. From the graph, it is observed that as the pH increases, the efficiency of MB removal also increases and the same trend is also observed as the increased dosage the removal efficiency also increases; this is due to the existence of a sulfonate group in MB and H^+ in acid solution. H^+ of acidic conditions will combine with the sulfonate group, decreasing the adsorption capacity [52]. As the pH value is lower, more H^+ is present in the solution, and thus, the adsorption capacity and percentage removal will be decreased. Lower removal was observed at lower pH due to competitive interactions of H+ and catatonic MB and the repulsive force interaction of the dye cations with the +ve surface of GO/CS. While rising solution pH (3-5), increased adsorptive removal of MB due to the number of –ve charged sites

enlarged that lead to the existence of the electrostatic force of attraction between cationic MB and GO/CS.

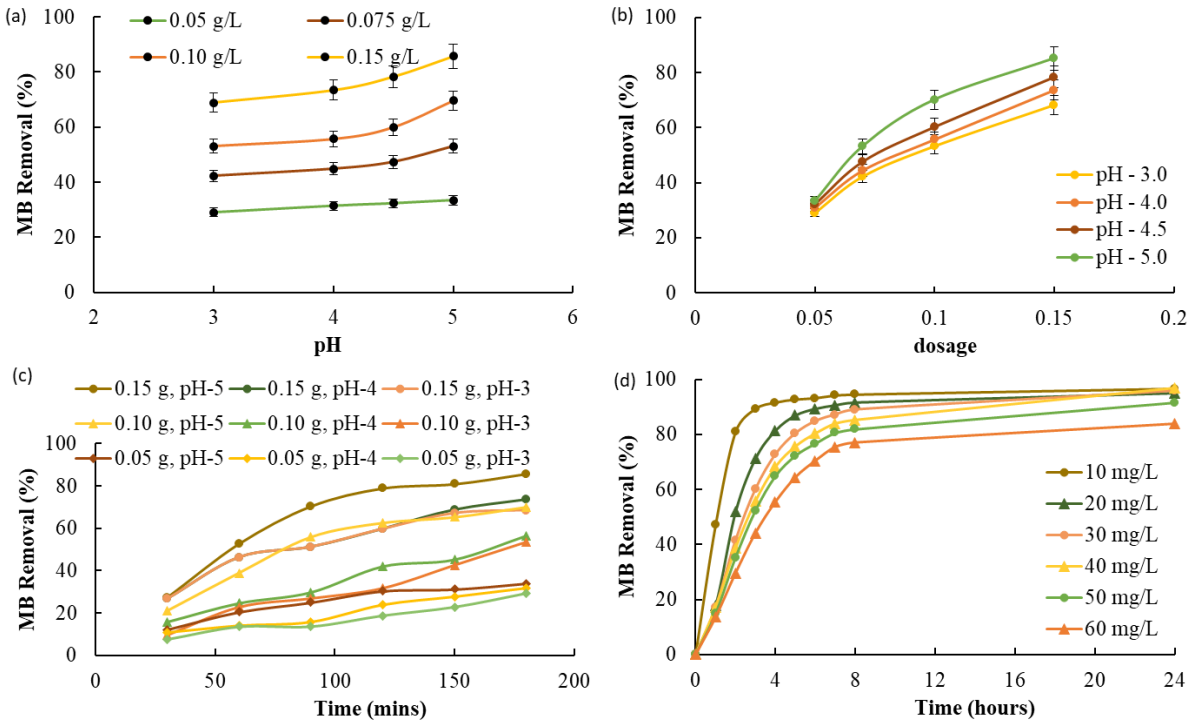

Figure 5: The behaviour of MB removal due to (a) pH at different dosage (b) dosages at different pH, (c) contact time at different dosages, and pH (d) contact time at different initial concentrations [Experiment conducted at the optimal conditions: pH of 5, adsorbent dosage: of 0.143 g/L and contact time of 125 min].

3.2.2 Effect of Dosage

Similar to the effect of pH, four different amounts of adsorbent dosage and four different pH were used to remove methylene dye over three hours. The percentage removal and adsorption capacity of the adsorbent were calculated and recorded every day for 30 min. The results of the study of dosage at different pH are shown in ***Figure 5 (b)***. From the graphs, it is noticeable that the increase in adsorbent dosage improves the dye removal efficiency (average) by 25% for every increase in pH value in the range of 3-5. The increase of percentage removal with adsorbent dosage is because of the increase in total active sites to adsorb the dye particles [45, 53].

3.2.3 Effect of Contact time

A graph percentage versus time with the combination of pH and dosage is plotted, as shown in ***Figure 5 (c)***. From the graph, the percentage removal increases over time, and the highest percentage removal is 85% with 0.15 g adsorbent at a pH of 5. The increase in percentage removal becomes lower after two hours. This is due to the active sites of the adsorbent being occupied, and the adsorbent starts to become saturated [45]. The difference in the increase in percentage removal became to be evident after 60 min for 0.05 g and 0.15 g adsorbent. When comparing the percentage removal at 180 min, 0.05 g adsorbent at pH of 3, 4, and 5 seem to reach their maximum adsorption as the adsorbate fully occupied the adsorbent. However, the line of 0.10 g and 0.15 g adsorbent with pH of 3, 4, and 5 are still increasing, and their maximum adsorption amount is yet to reach.

3.2.4 Effect of Initial Concentration

The initial concentration effect was investigated from 10 to 60 mg/L of methylene blue, as shown in ***Figure 5 (d)***. The amount of adsorbent used and pH of dye solution was set to 0.15g and pH of 5 as a result of the effect of pH and effect of adsorbent dosage show this condition has better efficiency in dye removal. The dye solution's concentration was checked every hour for 8 h, and an additional concentration reading was taken at 24 h to identify the equivalent adsorption amount. The highest adsorption capacity observed in this experiment is 16.7 mg/g, as seen in ***Figure 6***. For 10 mg/L dye solution, the adsorption amount has reached equilibrium at the third hour, while for 40 mg/L and above has yet to reach equilibrium after 8 h. A longer contact time is needed for a higher concentration of dye solution to remove the dye particles in the solution entirely. The equilibrium adsorption capacity indicates that the dye particles fully occupied the active sites of the adsorbent; more amount of adsorbent is needed to remove the remaining dye particles in the solution.

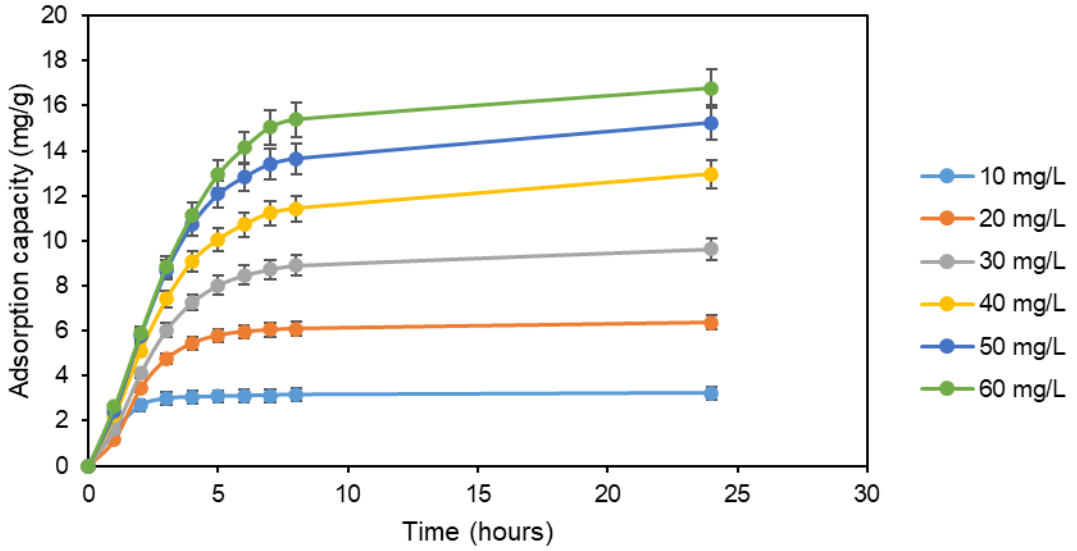

Figure 6: Effect of contact time on MB adsorption capacity at a different initial concentration. [Experiment conducted at the optimal conditions: pH of 5, adsorbent dosage: of 0.143 g/L and contact time of 125 min]

3.3 Interaction effects within process variables and their effect on MB removal (%)

In the above section, the effect of each process variable on the overall MB removal is investigated. However, each process variable may exhibit different behavior in the presence of other variables. The results are shown in **Figure 5** exhibit the behaviour of isotherm at the different concentrations for MB removal for the effect of pH, dosage and time. To understand the interactive effects within the process variables, 3D surface plots and contours, are drawn, as shown in **Figure 7**. It is observed that increasing the pH increases the time as results increase in MB removal was observed. Also, the contour plots shown on the bottom surface are distinctive, thus depicting the non-linear distribution within the process variables. **Figure 7** (***a***) depicts the 2D contour plot pH-and contact time on MB removal. The wider contours indicate the strong interaction between these factors. The 3D surface plot of the same combination of parameters is given in **Figure 7** (***b***). The curvature of the surface plot shows the interactive effect of pH – contact time on MB removal. It can be observed that the removal efficiency is very low at a lower contact time and lower pH. At lower contact time, higher pH is preferred

to obtain higher MB removal efficiency. The interactive effect of pH – dosage on MB removal is shown in **Figure 7** (***c***). It can be observed that the removal efficiency is increasing for different adsorbent dosages, irrespective of pH. At pH of 5 and dosage of 0.15 g/L, it results in removal efficiency of over 80%. The interactive effect of dosage-contact time on MB removal is shown in **Figure 7** (***d***). This interactive plot shows that higher dosage results in higher MB removal efficiency, irrespective of contact time.

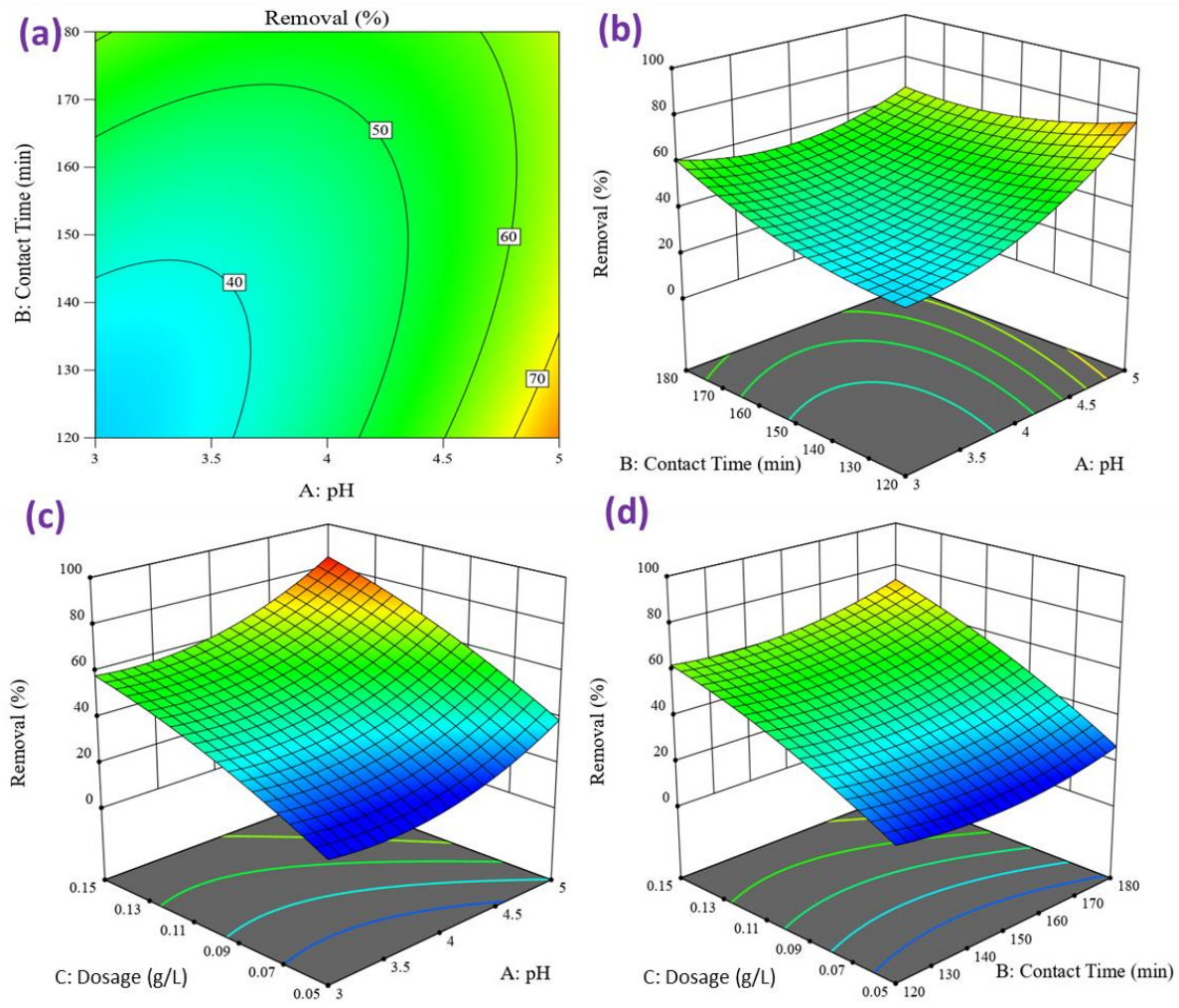

***Figure 7*:** (a) 2D contour plot pH-and contact time (b) 3D surface plots for MB removal-pH-contact time; (c) MB removal-pH-Dosage and (d) MB removal-contact time-Dosage

3.4 Multi-regression analysis

Conducting experiments at different process conditions is tedious and also involves lots of chemicals. Hence, conducting multiple experiments is expensive and leads to a waste of

chemicals. The DOE approach using RSM methodology is used to minimize the number of experiments. However, based on the minimum experiments conducted, it's good to develop a multi-regression relation that can be used to predict the MB removal efficiency at different process conditions. In this regard, ANOVA analysis (***see Table S1***) is used, and a quadratic expression for evaluation of removal (%) is obtained as follows:

$$\text{Removal (\%)} = +63.78 - 20.58 * pH - 0.717 * Time + 439.675 * Dosage - 0.307 * pH * Time + 28.70 * pH * Dosage + 1.295 * Time * Dosage + 9.451 * pH^2 + 0.0064 * Time^2 - 1600.50 * Dosage^2$$

Similarly, ANOVA analysis (***see Table S2***) is used and a quadratic expression for evaluation of adsorption amount is obtained as follows:

$$\text{Adsorption amount} = + 5.437 - 1.536 * pH - 0.053 * Time + 33.00 * Dosage - 0.027 * pH * Time + 2.10 * pH * Dosage + 0.096 * Time * Dosage + 0.701 * pH^2 + 0.0005 * Time^2 - 120.50 * Dosage^2$$

3.5 Implementation of ANN-PSO approach

As mentioned earlier, the identified process variables (pH, adsorbent dosage, and contact time) are used as inputs to the ANN-PSO framework, and response (MB removal %) is obtained as output from this model. The model is trained, tested, and validated using the 70%-15%-15% rule, in which the data is segregated randomly. The performance of ANN-PSO depends on various model parameters such as number of neurons, swarm size, cognition coefficient (C_1), and social assessment (C_2). Therefore, the optimal values of these parameters are evaluated, which are given in ***Table S3***. Also, the effect of the number of neurons in a hidden layer on the statistical metrics RMSE and R^2 is verified, as shown in ***Figure 8***. It can be seen that the eight neurons in the hidden layer are resulting in lower RMSE and higher R^2. Therefore, the 3-8-1 topology is considered an optimal ANN configuration. Accordingly, the optimal values of swarm size, C_1, and C_2 are estimated as shown in ***Table S3***, resulting in lower RMSE and higher

R^2. Finally, the optimal weights involved in the ANN-PSO framework were evaluated is given in ***Table S4***. Thus, the optimal ANN-PSO model values for the number of neurons, swarm size, maximum iterations, C_1 and C_2 are 8, 80, 300, 1.5, and 2.5, respectively.

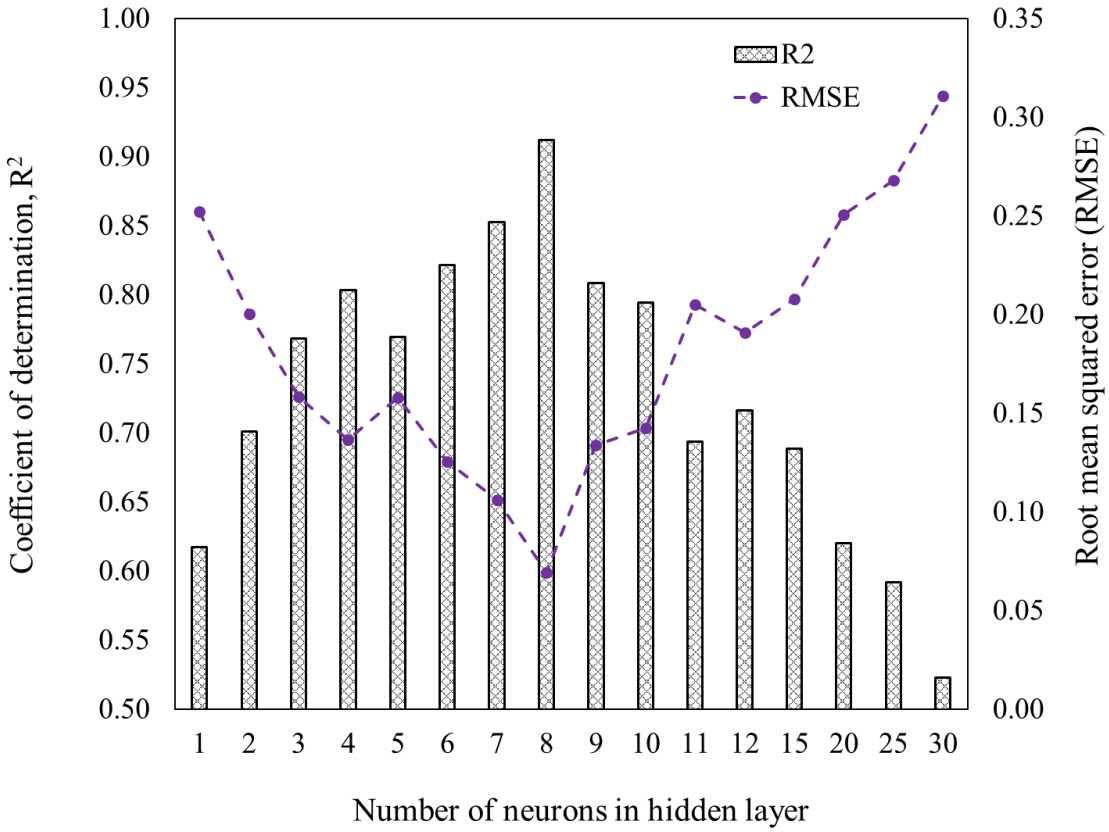

***Figure 8*:** Variation of RMSE and R^2 with respect to the number of neurons in the hidden layer

3.6 Comparison of RSM and ANN-PSO models

The effectiveness of the proposed approaches are validated to establish the superiority of the methods to depict the MB dye removal using GO/Ch composites. Therefore, the respective model (ANN-PSO and RSM) predictions are produced and compared, as shown in ***Figure 9***. It can be observed that both the model predictions are equally good; however, the ANN-PSO predictions are in good agreement with the experimental values compared to RSM predictions. Typically, the scatter plots are a good representation of model predictions, but they may not provide the complete picture of the goodness of fit or error distribution. Therefore, the model

predictions are compared by evaluating various statistical metrics. The various well-known nonlinear statistical metrics that can be used for validating the efficacy of model predictions are shown in ***Table 2***. It is found that the R^2 value for ANN-PSO is 0.998, which is much higher than the R^2 (0.981) of RSM. A similar trend is observed for all other metrics, thus confirming the superiority of ANN-PSO over RSM. Even though ANN-PSO is more computationally intensive than RSM, this model could capture the MB dye adsorption process characteristics.

Table 2. Nonlinear statistical metrics for validating the efficacy of model predictions

Error function	Mathematical expression	RSM	ANN-PSO
Coefficient of determination (R^2)	$\frac{\sum_{i=1}^{n}\left(\%R_{pred}^{i}-\%R_{exp}^{i}\right)^2}{\sum_{i=1}^{n}\left[\left(\%R_{pred}^{i}-\%R_{mean,exp}^{i}\right)^2\right]}$	0.981	0.998
Sum of the squares of errors (SSE)	$\sum_{i=1}^{n}\left(\%R_{pred}^{i}-\%R_{exp}^{i}\right)^2$	94.228	8.937
Average relative errors (ARE)	$\frac{100}{p}\sum_{i=1}^{n}\frac{\left\|\%R_{pred}^{i}-\%R_{exp}^{i}\right\|}{\%R_{exp}^{i}}$	1.311	0.415
Root means square errors (RMSE)	$\sqrt{\frac{1}{n-1}\sum_{i=1}^{n}\left(\%R_{pred}^{i}-\%R_{exp}^{i}\right)^2}$	2.427	0.747
Sum of the absolute errors (SAE)	$\sum_{i=1}^{n}\left\|\%R_{pred}^{i}-\%R_{exp}^{i}\right\|$	26.180	7.647
Absolute average deviation (AAD)	$\left\|\frac{1}{n}\sum_{i=1}^{n}\frac{\left(\%R_{pred}^{i}-\%R_{exp}^{i}\right)}{\%R_{exp}^{i}}\right\| * 100$	0.043	0.030
Pearson's Chi-square (χ^2)	$\chi^2=\sum_{i=1}^{n}\frac{\left(\%R_{pred}^{i}-\%R_{exp}^{i}\right)^2}{\%R_{\exp}^{i}}$	2.338	0.278
Marquart's percentage standard deviation (MPSD)	$100 * \sqrt{\frac{1}{n-p}\sum_{i=1}^{n}\frac{\left(\%R_{pred}^{i}-\%R_{exp}^{i}\right)^2}{\%R_{exp}^{i}}}$	15.705	1.925
Hybrid fractional error function (HYBRID)	$\frac{100}{n-p}\sum_{i=1}^{n}\frac{\left(\%R_{pred}^{i}-\%R_{exp}^{i}\right)^2}{\%R_{exp}^{i}}$	39.482	13.607

Where $q_{e,exp}^{i}, q_{e,pred}^{i}$ are the q_e values of the experimental and predicted values, respectively; *p* is the number of parameters; *n* is the number of experimental runs.

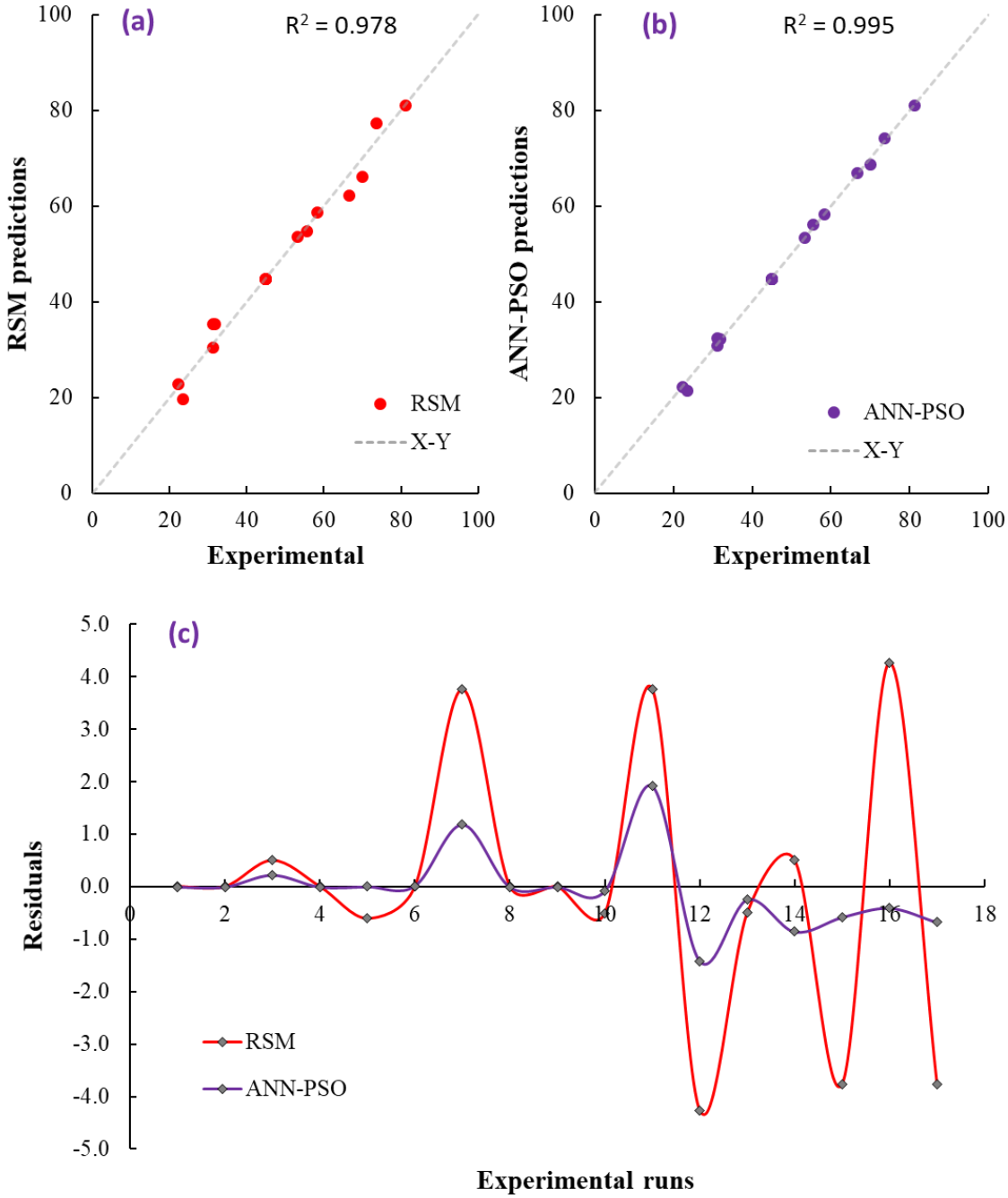

***Figure 9*: Assessment of RSM and ANN-PSO model predictions**

3.7 Adsorption Isotherms

To understand the inherent mechanisms of the MB adsorption process, different types of isotherm models are validated (see ***Table S5***). Most researchers linearize the non-linear isotherm models to estimate the respective isotherm parameters by fitting a regression line. But this linearization procedure underestimates the mechanisms involved in the adsorption process [54, 55]. So, a non-linear approach is implemented to estimate the respective isotherms, as shown in ***Table 3***. It can be observed that the non-linear approach gives higher R^2 than the linear approach for all isotherm models, indicating that this non-linear approach model better captures the non-linearity in the respective models. It can be observed that the R^2 values for all the considered isotherms are higher than 0.95, but the Freundlich isotherm model better depicts the MB adsorption by graphene oxide/chitosan composite, which gives $R^2 = 0.995$ and also lower statistical metrics. These results are very similar to other published works on MB adsorption [56]. To visualize the efficacy of the model parameters evaluated by the non-linear approach, these parameters (both linear and non-linear) are substituted in respective isotherm models, and q_e values are predicted. Various isotherm plots depicting linear and non-linear approaches are shown in ***Figure S4***. These plots also confirm that the parameters evaluated by the non-linear approach provide better predictions and are close to experimental values.

3.8 Kinetic modelling

To understand the inherent kinetic mechanism involved in MB adsorption using graphene oxide/chitosan composites, various adsorption reaction kinetic models (Pseudo first and second-order) and intraparticle diffusion kinetic models (Weber-Morris and Boyd) are investigated (see ***Table S6***). As mentioned in the previous section, most researchers also linearize the non-linear kinetic models to estimate the respective kinetic model parameters by fitting a regression line. But this linearization procedure underestimates the mechanisms involved in the adsorption process [54, 55]. So, the non-linear approach is implemented to

estimate the respective isotherms, as shown in ***Units:*** q_e (mg/g), K_1 (min^{-1}), K_2 (g mg^{-1} min^{-1}), K_{id} (mg/g $min^{0.5}$), B (min^{-1}) . Here the respective rate constants and equilibrium adsorption capacities were evaluated by both approaches. Since R^2 is the most occasionally used metric to identify the best kinetic model that can depict the inherent mechanism accordingly, R^2 is evaluated for all the investigated kinetic models for both linear and non-linear approaches. It can be observed that the R^2 value is higher for parameters evaluated by non-linear approaches. This itself signifies that the non-linear approach better captures the non-linearity in the kinetic model and hence better interprets the inherent mechanisms. It can be observed that Pseudo's first kinetic order provided an R^2 value of 0.9881, indicating that this model better explains the MB adsorption process. Hence, this adsorption system follows the Pseudo-first-order kinetic model [56].

To further visualize the efficacy of the kinetic model parameters evaluated by the non-linear approach, these parameters (both linear and non-linear) are substituted in respective kinetic models, and corresponding adsorption capacity at equilibrium (qe) values are predicted. Various kinetic model plots depicting linear and non-linear approaches are shown in Figure S3. These plots also confirm that the parameters evaluated by the non-linear approach provide better predictions and are close to experimental values.

Table 3. *Validation of various Isotherm models for depicting MB adsorption by graphene oxide/chitosan composite*

Models →	**Freundlich**		**Langmuir**		**Temkin**		**Redlich–Peterson**		**Sips**		**Toth**	
Statistical metrics ↓	**Linear**	**Non-linear**	**Linear**	**Non-linear**	**Linear**	**Non-linear**	**Linear**	**Non-linear**	**Linear**	**Non-linear**	**Linear**	**Non-linear**
Parameters →	K_F: 6.54 b_F: 1.727	K_F: 6.79 b_F: 1.833	K_L: 18.55 b_L: 0.67	K_L: 25.35 b_L: 0.35	b_T: 4.72 K_T: 5.143	b_T: 4.86 K_T: 4.948	K_R: 12.58 a_R: 0.715 α: 0.941	K_R: 11.99 a_R: 0.774 α: 0.777	K_s: 22.29 b_s: 0.476 n_s: 1.127	K_s: 33.88 b_s: 0.247 n_s: 1.228	K_{th}: 31.26 b_{th}: 0.331 n_{th}: 0.823	K_{th}: 43.51 b_{th}: 0.528 n_{th}: 0.57
R^2	0.991	0.995	0.956	0.983	0.945	0.948	0.966	0.986	0.972	0.987	0.979	0.986
SAE	1.833	1.651	4.975	2.656	5.158	5.018	4.352	2.607	4.116	2.492	5.059	2.519
SSE	1.403	1.219	6.513	1.944	5.700	5.619	4.738	1.496	4.478	1.405	6.376	1.510
ARE	7.281	6.594	23.598	6.062	36.652	35.876	21.481	9.274	19.158	9.086	34.039	10.283
RMSE	0.592	0.474	1.276	0.497	1.194	1.106	1.088	0.632	1.058	0.593	1.263	0.614

Units: Langmuir: K_L (mg/g), b_L (L/mg); Freundlich: K_F ($mg^{-1-(1/n)}\,L^{(1/n)}\,g^{-1}$), b_F is dimensionless; Temkin: K_T (L/mg), b_T (J/mol); Redlich–Peterson: K_R (L/g), a_R(L/mg) ^{nP}, n_R is dimensionless; Sips: K_S (mg/g), b_s $(L/mg)^n$, n_s is dimensionless; Toth: K_{th} (L/g), b_{th} $(mg/L)^n$, n_{th} is dimensionless.

Table 4. *Validation of various Kinetic models for depicting MB adsorption by graphene oxide/chitosan composite*

Models →	Pseudo first order		Pseudo-second-order		**Weber - Morris**		**Boyd**	
Statistical metrics ↓	**Linear**	**Non-linear**	**Linear**	**Non-linear**	**Linear**	**Non-linear**	**Linear**	**Non-linear**
Parameters →	K_1: 0.015 q_e: 3.153	K_1: 0.013 q_e: 3.190	K_2: 0.023 q_e: 4.356	K_2: 0.004 q_e: 3.862	K_{id}:0.1997	K_{id}:0.1915	B: 0.0144 q_e: 3.106	B: 0.0114 q_e: 2.990
R^2	0.9811	0.9881	0.8823	0.9388	0.7496	0.7624	0.9570	0.9747
SAE	7.757	6.732	12.099	10.848	33.007	31.350	25.710	28.563
SSE	0.098	0.068	0.263	0.167	0.955	0.869	0.555	0.407
ARE	0.488	0.330	1.069	0.894	1.934	1.917	0.859	1.168
RMSE	0.140	0.116	0.229	0.183	0.437	0.385	0.333	0.285

Units: q_e (mg/g), K_1 (min^{-1}), K_2 (g mg^{-1} min^{-1}), K_{id} (mg/g $min^{0.5}$), B (min^{-1})

3.9 Process optimization and model validation

To identify the optimal process variables at which maximum MB removal efficiency and adsorption amount are obtained, the above discussed RSM approach is implemented. The respective process conditions for maximum MB removal efficiency and adsorption amount are shown in ***Table 5***. The developed ANN-PSO data-driven model is implemented to predict both responses based on these optimal process conditions. Experiments are conducted at these process conditions, and respective MB removal efficiency and adsorption amount obtained are tabulated in this table.

It was observed that the ANN-PSO and RSM model-based predictions are in good agreement with obtained experimental values (standard deviation of less than 2%); however, the ANN-PSO model predictions are very close to experimental values. These results further confirm that the ANN-PSO-based approach can capture the inherent mechanisms of the MB adsorption process and can be used as a good modelling approach. **Table 6** compares the removal efficiency of MB dye with different adsorbents. It can be observed that the GO/CS has resulted in higher MB dye removal and lowest adsorption capacity, compared to other adsorbents. It can also be observed that the dye removal adsorption experiments resulted in high removal efficiency at a pH of 5.

Table 5. Comparison of maximum MB removal efficiency by RSM and ANN-PSO at the optimal conditions & initial dye concentration of 10mg/L.

No	A	B	C	Response		
	pH	Dosage (g/L)	Contact Time (min)	Expt.	RSM Pred.	ANN-PSO Pred.
				Removal Efficiency (%)		
1	5.0	0.143	124.9	90.34	90.02	90.28
2	4.9	0.149	122.0	88.67	88.40	88.60

Table 6. Comparison of removal efficiency of MB dye with different adsorbents

Adsorbent	pH	Removal efficiency (%)	Adsorption capacity mg/g	References
Hydroxypropyl cellulose/ GO	-	>70	27.849	
Raw mango seed	5	80	25.36	
Cobalt-benzene-1,3,5-tricarboxylate	8	67	58	
Tea waste-based activation carbon based on chemical activation agent (H_3PO_4, KOH and $ZnCl_2$)	-	70	238.1 357.14 147.06	
copper-benzene-1,3,5-tricarboxylate	5	84	288.72	
Coconut shell-biochar	10	88.01	-	
Alginate polymer modified with pandan leaves	5	61	-	
Graphene oxide-potato starch	8	80	500	
Cu-doped-Fe-Benzene dicarboxylic acid metal organic framework	5	82	8.56 - 23.92	
CS nano-montmorillonite The produced composite was named R0, RI, RII, and RIII for montmorillonite ratios zero, 0.05, 0.07, and 0.10, respectively	8	88.47	248.9, 276.03, 204.39, and 180	
GO/CS	5	90.34	7.53	Present study

4. Conclusions

This research study is mainly focused on synthesizing graphene oxide/chitosan composite and determining its feasibility for MB dye removal. The fabrication of the composites was successful and was proven by the characterization via FTIR, SEM, EDX, and TGA. The functional groups of epoxy, carbonyl, and hydroxyl were found in GO and GO/CS composites, while the amide functional group was found in GO/CS composites. At acidic conditions, the dye removal application has shown higher efficiency at a high pH value. The adsorption

capacity is considered low, and this might be due to the agglomeration of the adsorbent in the dye solution, which decreases the contact area between dye particles and adsorbents. The ANOVA results for the quadratic models obtained for predicting MB removal (%) and the adsorption amount were found that the model is very significant, which resulted in a p-value of 0.0014. ANN-PSO framework is implemented to obtain the data-driven model. The optimal ANN-PSO model values for the number of neurons, swarm size, maximum iterations, C_1 and C_2 are 8, 80, 300, 1.5 and 2.5, respectively. ANN-PSO predictions are in good agreement with the experimental values and hence resulted in higher R^2 (=0.998) compared to RSM predictions (R^2 = 0.981). The maximum MB removal efficiency (90.34%) and adsorption amount (7.53 mg/g) can be obtained at an initial dye concentration of 10 mg/L and optimal values of pH (5), adsorbent dosage (0.143 g/L) and contact time (125 min).

Funding: This section is Not applicable

Acknowledgments: Authors would like to acknowledge the finical support provided by Taif University Researchers Supporting Project Number (TURSP-2020/106).

Competing interests: The authors declare no conflict of interest.

Availability of data and materials: Data is available on personal request.

Author Contributions: N.M. Mubarak, Rama Rao Karri designed the research; Goh Kheng Khiam performed Experimental work; Mohammad Khalid, Rashmi Walvekar, and Ezzat Chan Abdullah did data analysis. N.M. Mubarak, Rama Rao Karri, Mohammad Khalid, and Goh Kheng Khiam wrote the manuscript.

References

1. Karri, R.R., Ravindran, G., and Dehghani, M.H., (2021) *Wastewater—Sources, Toxicity, and Their Consequences to Human Health*, in *Soft Computing Techniques in Solid Waste and Wastewater Management*. Elsevier. p. 3-33. https://doi.org/10.1016/B978-0-12-824463-0.00001-X
2. Solís, M., Solís, A., Pérez, H.I., Manjarrez, N., and Flores, M., (2012). Microbial decolouration of azo dyes: A review. *Process Biochemistry (Amsterdam, Netherlands)*. 47(12): 1723-1748. DOI: https://doi.org/10.1016/j.procbio.2012.08.014.

3. Singha, K., Pandit, P., Maity, S., and Sharma, S.R., (2021) *Chapter 11 - Harmful environmental effects for textile chemical dyeing practice*, in *Green Chemistry for Sustainable Textiles*, N. Ibrahim and C.M. Hussain, Editors., Woodhead Publishing. p. 153-164. https://doi.org/10.1016/B978-0-323-85204-3.00005-1
4. Bank, W., (2007) *Environmental, health, and safety guidelines for tanning and leather finishing.*

Group. IFC E&S. Washington, D.C. : World Bank.
5. Bhatia, D., Sharma, N.R., Singh, J., and Kanwar, R.S., (2017). Biological methods for textile dye removal from wastewater: A review. *Critical Reviews in Environmental Science and Technology*. 47(19): 1836-1876. DOI: https://doi.org/10.1080/10643389.2017.1393263.
6. Kandisa, R.V. and Saibaba KV, N., (2016). Dye Removal by Adsorption: A Review. *Journal of Bioremediation & Biodegradation*. 07(06): 371. DOI: https://doi.org/10.4172/2155-6199.1000371.
7. Rai, Prabhat K., Lee, J., Kailasa, S.K., Kwon, E.E., Tsang, Y.F., Ok, Y.S., and Kim, K.-H., (2018). A critical review of ferrate(VI)-based remediation of soil and groundwater. *Environmental Research*. 160: 420-448. DOI: https://doi.org/10.1016/j.envres.2017.10.016.
8. Ambade, B., Sethi, S.S., Kurwadkar, S., Kumar, A., and Sankar, T.K., (2021). Toxicity and health risk assessment of polycyclic aromatic hydrocarbons in surface water, sediments and groundwater vulnerability in Damodar River Basin. *Groundwater for Sustainable Development*. 13: 100553. DOI: https://doi.org/10.1016/j.gsd.2021.100553.
9. Pradhan, S.K., Ambade, B., and Tarafder, P.K., (2020). An evolved fluorimetric determination of uranium in rock/mineral sample solutions containing hydrolysable elements such as Nb, Ta, Zr and Ti sequestered by bi-fluoride. *Applied Radiation and Isotopes*. 160: 109126. DOI: https://doi.org/10.1016/j.apradiso.2020.109126.
10. Ballav, N., Das, R., Giri, S., Muliwa, A.M., Pillay, K., and Maity, A., (2018). l-cysteine doped polypyrrole (PPy@L-Cyst): A super adsorbent for the rapid removal of Hg+2 and efficient catalytic activity of the spent adsorbent for reuse. *Chemical Engineering Journal*. 345: 621-630. DOI: https://doi.org/10.1016/j.cej.2018.01.093.
11. Manavi, N., Kazemi, A.S., and Bonakdarpour, B., (2017). The development of aerobic granules from conventional activated sludge under anaerobic-aerobic cycles and their adaptation for treatment of dyeing wastewater. *Chemical Engineering Journal*. 312: 375-384. DOI: https://doi.org/10.1016/j.cej.2016.11.155.
12. Mojsov, K., Andronikov, D., Janevski, A., Kuzelov, A., and Gaber, S., (2016). The application of enzymes for the removal of dyes from textile effluents. *Advanced technologies*. 5(1): 81-86. DOI: https://doi.org/10.5937/savteh1601081m.
13. Lingamdinne, L.P., Koduru, J.R., and Karri, R.R., (2019). A comprehensive review of applications of magnetic graphene oxide based nanocomposites for sustainable water purification. *Journal of Environmental Management*. 231: 622-634. DOI: 10.1016/j.jenvman.2018.10.063.
14. Koduru, J.R., Karri, R.R., and Mubarak, N.M., (2019) *Smart Materials, Magnetic Graphene Oxide-Based Nanocomposites for Sustainable Water Purification*, in *Sustainable Polymer Composites and Nanocomposites*. Springer International Publishing. p. 759-781.
15. Cheaburu-Yilmaz, C.N., Yilmaz, O., and Vasile, C., (2015) *Eco-Friendly Chitosan-Based Nanocomposites: Chemistry and Applications*, in *Advanced Structured Materials*. Springer India. p. 341-386.

16. Radamson, H.H., (2017) *Graphene*, in *Springer Handbook of Electronic and Photonic Materials*. Springer International Publishing. p. 1. https://doi.org/10.1007/978-3-319-48933-9_48
17. Lingamdinne, L.P., Koduru, J.R., Chang, Y.-Y., and Karri, R.R., (2018). Process optimization and adsorption modeling of Pb(II) on nickel ferrite-reduced graphene oxide nano-composite. *Journal of Molecular Liquids*. 250: 202-211. DOI: https://doi.org/10.1016/j.molliq.2017.11.174.
18. Lim, J.Y., Mubarak, N.M., Abdullah, E.C., Nizamuddin, S., Khalid, M., and Inamuddin, (2018). Recent trends in the synthesis of graphene and graphene oxide based nanomaterials for removal of heavy metals — A review. *Journal of Industrial and Engineering Chemistry*. 66: 29-44. DOI: https://doi.org/10.1016/j.jiec.2018.05.028.
19. Shamshina, J.L., Berton, P., and Rogers, R.D., (2019). Advances in Functional Chitin Materials: A Review. *ACS Sustainable Chemistry & Engineering*. 7(7): 6444-6457. DOI: 10.1021/acssuschemeng.8b06372.
20. Duan, B., Huang, Y., Lu, A., and Zhang, L., (2018). Recent advances in chitin based materials constructed via physical methods. *Progress in Polymer Science*. 82: 1-33. DOI: 10.1016/j.progpolymsci.2018.04.001.
21. Dehghani, M.H., Ghadermazi, M., Bhatnagar, A., Sadighara, P., Jahed-Khaniki, G., Heibati, B., and McKay, G., (2016). Adsorptive removal of endocrine disrupting bisphenol A from aqueous solution using chitosan. *Journal of Environmental Chemical Engineering*. 4(3): 2647-2655. DOI: https://doi.org/10.1016/j.jece.2016.05.011.
22. Rasoulzadeh, H., Dehghani, M.H., Mohammadi, A.S., Karri, R.R., Nabizadeh, R., Nazmara, S., Kim, K.-H., and Sahu, J.N., (2019). Parametric modelling of Pb (II) adsorption onto chitosan-coated Fe3O4 particles through RSM and DE hybrid evolutionary optimization framework. *Journal of Molecular Liquids*. 111893. DOI: https://doi.org/10.1016/j.molliq.2019.111893.
23. Vo, T.S., Vo, T.T.B.C., Suk, J.W., and Kim, K., (2020). Recycling performance of graphene oxide-chitosan hybrid hydrogels for removal of cationic and anionic dyes. *Nano convergence*. 7(1): 4-4. DOI: https://doi.org/10.1186/s40580-019-0215-0.
24. El Achaby, M., Essamlali, Y., El Miri, N., Snik, A., Abdelouahdi, K., Fihri, A., Zahouily, M., and Solhy, A., (2014). Graphene oxide reinforced chitosan/polyvinylpyrrolidone polymer bio-nanocomposites. *Journal of Applied Polymer Science*. 131(22). DOI: https://doi.org/10.1002/app.41042.
25. Sabzevari, M., Cree, D.E., and Wilson, L.D., (2018). Graphene Oxide–Chitosan Composite Material for Treatment of a Model Dye Effluent. *ACS Omega*. 3(10): 13045-13054. DOI: 10.1021/acsomega.8b01871.
26. Muda, M.S., Kamari, A., Bakar, S.A., Yusoff, S.N.M., Fatimah, I., Phillip, E., and Din, S.M., (2020). Chitosan-graphene oxide nanocomposites as water-solubilising agents for rotenone pesticide. *Journal of Molecular Liquids*. 318: 114066. DOI: https://doi.org/10.1016/j.molliq.2020.114066.
27. Sahu, J.N., Gangadharan, P., and Meikap, B.C., (2011). Optimization process parameters for in-situ synthesis of ammonia by catalytic hydrolysis of urea with fly ash in a batch reactor for safe feedstock in power plants. *Journal of Environmental Science and Health, Part A*. 46(8): 874-886. DOI: https://doi.org/10.1080/10934529.2011.580200.
28. Lingamdinne, L.P., Vemula, K.R., Chang, Y.-Y., Yang, J.-K., Karri, R.R., and Koduru, J.R., (2020). Process optimization and modeling of lead removal using iron oxide nanocomposites generated from bio-waste mass. *Chemosphere*. 243: 125257. DOI: https://doi.org/10.1016/j.chemosphere.2019.125257.

29. Puertas Arbizu, I. and Luis Pérez, C.J., (2003). Surface roughness prediction by factorial design of experiments in turning processes. *Journal of Materials Processing Technology*. 143-144: 390-396. DOI: https://doi.org/10.1016/s0924-0136(03)00407-2.
30. Ahmadi, S., Mesbah, M., Igwegbe, C.A., Ezeliora, C.D., Osagie, C., Khan, N.A., Dotto, G.L., Salari, M., and Dehghani, M.H., (2021). Sono electro-chemical synthesis of LaFeO3 nanoparticles for the removal of fluoride: Optimization and Modeling using RSM, ANN and GA tools. *Journal of Environmental Chemical Engineering*. 105320. DOI: https://doi.org/10.1016/j.jece.2021.105320.
31. Karri, R.R., Tanzifi, M., Tavakkoli Yaraki, M., and Sahu, J.N., (2018). Optimization and modeling of methyl orange adsorption onto polyaniline nano-adsorbent through response surface methodology and differential evolution embedded neural network. *Journal of Environmental Management*. 223: 517-529. DOI: https://doi.org/10.1016/j.jenvman.2018.06.027.
32. Jun, L.Y., Karri, R.R., Yon, L.S., Mubarak, N.M., Bing, C.H., Mohammad, K., Jagadish, P., and Abdullah, E.C., (2020). Modeling and optimization by particle swarm embedded neural network for adsorption of methylene blue by jicama peroxidase immobilized on buckypaper/polyvinyl alcohol membrane. *Environmental Research*. 183: 109158. DOI: 10.1016/j.envres.2020.109158.
33. Mohammadhassani, J., Dadvand, A., Khalilarya, S., and Solimanpur, M., (2015). Prediction and reduction of diesel engine emissions using a combined ANN–ACO method. *Applied Soft Computing*. 34: 139-150.
34. Jun, L.Y., Karri, R.R., Mubarak, N.M., Yon, L.S., Bing, C.H., Khalid, M., Jagadish, P., and Abdullah, E.C., (2020). Modelling of methylene blue adsorption using peroxidase immobilized functionalized Buckypaper/polyvinyl alcohol membrane via ant colony optimization. *Environmental Pollution*. 259: 113940. DOI: https://doi.org/10.1016/j.envpol.2020.113940.
35. Du, K.-L. and Swamy, M.N.S., (2016) *Particle Swarm Optimization*, in *Search and Optimization by Metaheuristics*. Springer International Publishing. p. 153-173.
36. Jia, W. and Lu, S., (2014). Few-layered graphene oxides as superior adsorbents for the removal of Pb(II) ions from aqueous solutions. *Korean Journal of Chemical Engineering*. 31(7): 1265-1270. DOI: https://doi.org/10.1007/s11814-014-0045-z.
37. Lau, Y.J., Karri, R.R., Mubarak, N.M., Lau, S.Y., Chua, H.B., Khalid, M., Jagadish, P., and Abdullah, E.C., (2020). Removal of dye using peroxidase-immobilized Buckypaper/polyvinyl alcohol membrane in a multi-stage filtration column via RSM and ANFIS. *Environmental Science and Pollution Research*. 27(32): 40121-40134. DOI: 10.1007/s11356-020-10045-2.
38. Jua, L.Y., Karri, R.R., Mubarak, N.M., Yon, L.S., Bing, C.H., Khalid, M., Jagadish, P., and Abdullah, E.C., (2020). Modeling of methylene blue adsorption using functionalized Buckypaper/Polyvinyl alcohol membrane via ant colony optimization. *Environmental Pollution*. 259: 113940. DOI: 10.1016/j.envpol.2020.113940.
39. Karri, R.R. and Sahu, J.N., (2018). Modeling and optimization by particle swarm embedded neural network for adsorption of zinc (II) by palm kernel shell based activated carbon from aqueous environment. *Journal of Environmental Management*. 206: 178-191. DOI: 10.1016/j.jenvman.2017.10.026.
40. Ganesh, B.M., Isloor, A.M., and Ismail, A.F., (2013). Enhanced hydrophilicity and salt rejection study of graphene oxide-polysulfone mixed matrix membrane. *Desalination*. 313: 199-207. DOI: https://doi.org/10.1016/j.desal.2012.11.037.
41. Kosowska, K., Domalik-Pyzik, P., Nocuń, M., and Chłopek, J., (2018). Chitosan and graphene oxide/reduced graphene oxide hybrid nanocomposites – Evaluation of

physicochemical properties. *Materials Chemistry and Physics*. 216: 28-36. DOI: https://doi.org/10.1016/j.matchemphys.2018.05.076.

42. Zuo, P.-P., Feng, H.-F., Xu, Z.-Z., Zhang, L.-F., Zhang, Y.-L., Xia, W., and Zhang, W.-Q., (2013). Fabrication of biocompatible and mechanically reinforced graphene oxide-chitosan nanocomposite films. *Chemistry Central Journal*. 7(1): 39-39. DOI: https://doi.org/10.1186/1752-153X-7-39.
43. Shahriary, L., Ghourchian, H., and Athawale, A.A., (2014). Graphene-Multiwalled Carbon Nanotube Hybrids Synthesized by Gamma Radiations: Application as a Glucose Sensor. *Journal of Nanotechnology*. 2014: 1-10. DOI: https://doi.org/10.1155/2014/903872.
44. Cobos, M., González, B., Fernández, M.J., and Fernández, M.D., (2017). Chitosan-graphene oxide nanocomposites: Effect of graphene oxide nanosheets and glycerol plasticizer on thermal and mechanical properties. *Journal of Applied Polymer Science*. 134(30): 45092. DOI: https://doi.org/10.1002/app.45092.
45. Guo, X., Qu, L., Tian, M., Zhu, S., Zhang, X., Tang, X., and Sun, K., (2016). Chitosan/Graphene Oxide Composite as an Effective Adsorbent for Reactive Red Dye Removal. *Water Environment Research*. 88(7): 579-588. DOI: https://doi.org/10.2175/106143016x14609975746325.
46. Zhang, J., Yang, H., Shen, G., Cheng, P., Zhang, J., and Guo, S., (2010). Reduction of graphene oxide vial-ascorbic acid. *Chem. Commun.* 46(7): 1112-1114. DOI: https://doi.org/10.1039/b917705a.
47. Thomas, R.T., Abdul Rasheed, P., and Sandhyarani, N., (2014). Synthesis of nanotitania decorated few-layer graphene for enhanced visible light driven photocatalysis. *Journal of Colloid and Interface Science*. 428: 214-221. DOI: https://doi.org/10.1016/j.jcis.2014.04.054.
48. Cai, Y., Wu, C., Liu, Z., Zhang, L., Chen, L., Wang, J., Wang, X., Yang, S., and Wang, S., (2017). Fabrication of a phosphorylated graphene oxide–chitosan composite for highly effective and selective capture of U(vi). *Environmental Science: Nano*. 4(9): 1876-1886. DOI: https://doi.org/10.1039/c7en00412e.
49. Han, D., Yan, L., Chen, W., and Li, W., (2011). Preparation of chitosan/graphene oxide composite film with enhanced mechanical strength in the wet state. *Carbohydrate Polymers*. 83(2): 653-658. DOI: https://doi.org/10.1016/j.carbpol.2010.08.038.
50. Sabzevari, M., Cree, D.E., and Wilson, L.D., (2018). Graphene Oxide-Chitosan Composite Material for Treatment of a Model Dye Effluent. *ACS Omega*. 3(10): 13045-13054. DOI: https://doi.org/10.1021/acsomega.8b01871.
51. El Rouby, W.M.A., Farghali, A.A., Sadek, M.A., and Khalil, W.F., (2018). Fast Removal of Sr(II) From Water by Graphene Oxide and Chitosan Modified Graphene Oxide. *Journal of Inorganic and Organometallic Polymers and Materials*. 28(6): 2336-2349. DOI: https://doi.org/10.1007/s10904-018-0885-9.
52. Fan, L., Luo, C., Li, X., Lu, F., Qiu, H., and Sun, M., (2012). Fabrication of novel magnetic chitosan grafted with graphene oxide to enhance adsorption properties for methyl blue. *Journal of Hazardous Materials*. 215-216: 272-279. DOI: https://doi.org/10.1016/j.jhazmat.2012.02.068.
53. Etim, U.J., Umoren, S.A., and Eduok, U.M., (2016). Coconut coir dust as a low cost adsorbent for the removal of cationic dye from aqueous solution. *Journal of Saudi Chemical Society*. 20: S67-S76. DOI: https://doi.org/10.1016/j.jscs.2012.09.014.
54. Karri, R.R., Sahu, J.N., and Jayakumar, N.S., (2017). Optimal isotherm parameters for phenol adsorption from aqueous solutions onto coconut shell based activated carbon: Error analysis of linear and non-linear methods. *Journal of the Taiwan Institute of Chemical Engineers*. 80: 472-487. DOI: https://doi.org/10.1016/j.jtice.2017.08.004.

55. Dehghani, M.H., Karri, R.R., Yeganeh, Z.T., Mahvi, A.H., Nourmoradi, H., Salari, M., Zarei, A., and Sillanpää, M., (2020). Statistical modelling of endocrine disrupting compounds adsorption onto activated carbon prepared from wood using CCD-RSM and DE hybrid evolutionary optimization framework: Comparison of linear vs non-linear isotherm and kinetic parameters. *Journal of Molecular Liquids*. 302: 112526. DOI: https://doi.org/10.1016/j.molliq.2020.112526.
56. Savcı, S. and Mert Uysal, M., (2017) *Adsorption of Methylene Blue and Methyl Orange By Using Waste Ash*. Vol. 21. 10.